Acta Crystallographica Section D
**Biological Crystallography**
ISSN 0907-4449

# Structure of sylvaticin, a new $\alpha$-elicitin-like protein from *Pythium sylvaticum*

**Marie-Bernard Lascombe,[a]* Pascal Retailleau,[b] Michel Ponchet,[c] Benoît Industri,[c] Jean-Pierre Blein[d] and Thierry Prangé[a]**

[a]Laboratoire de Cristallographie et RMN Biologiques, Université Paris Descartes, UMR 8015 CNRS, Faculté de Pharmacie, 4 Avenue de l'Observatoire, 75006 Paris, France, [b]Service de Cristallochimie, Institut de Chimie des Substances Naturelles–CNRS, Bâtiment 27, 1 Avenue de la Terrasse, 91198 Gif sur Yvette CEDEX, France, [c]UMR Interactions Plantes–Microorganismes et Santé Végétale, INRA, 400 Route des Chappes, BP 167, 06903 Sophia Antipolis CEDEX, France, and [d]Phytopharmacie, UMR 692 CNRS, INRA, Domaine d'Époisses, BP 86510, 21065 Dijon CEDEX, France

Correspondence e-mail: marie-bernard.lascombe@univ-paris5.fr

Received 14 July 2007
Accepted 4 September 2007

**PDB References:** sylvaticin, 2pos, r2possf; 2pr0, r2pr0sf.

The structure of sylvaticin, a 10 kDa major pythin protein excreted by the parasitic oomycete *Pythium sylvaticum*, has been determined. Although closely related to $\alpha$-elicitins in its biological response, toxicity and overall structure, sylvaticin presents a number of structural features that make it an unusual member of the elicitin class. Elicitins possess a large hydrophobic cavity and the mechanism of the systemic acquired resistance induced *in planta* is known to proceed through lipid transport and complexation within this cavity. Unlike other elicitins, sylvaticin contains tryptophan residues, one of which points inwards towards the central cavity, thus limiting access to sterols. In the case of sylvaticin, the sterol-transport mechanism is likely to be of less importance compared with other members of the elicitin family and still remains to be fully characterized.

## 1. Introduction

Among the oomycetes, the phytopathogenic *Phytophthora* and *Pythium* spp. are distributed worldwide and cause severe damage to economically important crops both in temperate and tropical areas. They secrete small 10 kDa proteins that in some plants, especially tobacco, can induce tissue necrosis (hypersensitive-like response; HR) shortly followed by a systemic acquired resistance (SAR) against a wide range of pathogens. These extracellular proteins can be divided into two groups depending on their pI ($\alpha$- and $\beta$-elicitins). The basic proteins ($\beta$-elicitins) are more necrotizing than the acidic proteins ($\alpha$-elicitins; Ponchet *et al.*, 1999). All elicitins investigated to date exhibit high sequence homology (up to 80%) and they all lack the three residue types histidine, arginine and tryptophan. The three-dimensional structure of cryptogein, a $\beta$-elicitin secreted by *Phytophthora cryptogea*, is now well documented both from X-ray (Boissy *et al.*, 1996) and NMR (Fefeu *et al.*, 1997; Gooley *et al.*, 1998) analyses. The structure of $\beta$-cinnamomin from *Phytophthora cinnamomi* (Rodrigues *et al.*, 2002) is nearly identical to that of cryptogein and confirms all the previous structural data. Elicitins also present additional properties and are able to load and transfer lipids and sterols (Mikes *et al.*, 1997, 1998). The three-dimensional structures of cryptogein–sterol complexes (Boissy *et al.*, 1999; Lascombe *et al.*, 2002) and the cinnamomin–ergosterol complex (Rodrigues *et al.*, 2006) provided interesting information on how the complex is formed and stabilized. These data were of prime importance in building mutated and engineered cryptogeins that suggested that the active form of

elicitins for SAR and HR induction is the elicitin–sterol complex (Mikes *et al.*, 1998; Osman *et al.*, 2001).

A small number of *Pythium* spp. have been reported to secrete proteins (named pythins) that show high homology to elicitins (Huet *et al.*, 1995; Panabières *et al.*, 1997), while some other *Pythium* spp. belonging to other phylogenetic clades (Wang & White, 1997) produce 10 kDa elicitin-like proteins that show new features such as low sequence homology with elicitins and the presence of tryptophan or arginine residues, which are not observed in elicitins (M. Ponchet & F. Panabières, personal communication). Together with elicitins, these pythins show interesting biological properties: the induction of SAR with only low HR symptoms (Picard *et al.*, 2000; Benhamou *et al.*, 2001; Le Floch *et al.*, 2005). To date, only oligandrin from *P. oligandrum* has been crystallized (Lascombe *et al.*, 2000), but its three-dimensional structure has not yet been solved owing to perfect hemihedral twinning. The present report concerns sylvaticin, another 10 kDa pythin secreted by *P. sylvaticum*, which is the first tryptophan-containing $\alpha$-elicitin-like protein (Fig. 1). Although relatively more toxic than oligandrin, sylvaticin presents interesting SAR features. The crystallization of sylvaticin has previously been reported in this journal (Lascombe *et al.*, 2004).

## 2. Materials and methods

### 2.1. Extraction and purification of sylvaticin

*P. sylvaticum* (strain 37 from INRA Antibes collection) was maintained on 1% malt/1% agar solid medium in 10 cm Petri dishes. 5–6 d old cultures were used to inoculate glucose/asparagine-based liquid medium as described previously (Bonnet *et al.*, 1996). After 8 d, the culture filtrate was recovered after filtration on a GF/C filter (Whatman) placed on a Büchner funnel and concentrated tenfold under vacuum in a rotary evaporator. The concentrated culture filtrate was dialyzed against ultrapure water (three times) and then adjusted to 5 m*M* sodium acetate/trifluoroacetic acid pH 4 and loaded onto a Macroprep High S (Bio-Rad) cation-exchange column pre-equilibrated with the same buffer. After washing with 5 m*M* sodium acetate/trifluoroacetic acid pH 4, elution was carried out with increasing amounts of NaCl (up to 1 *M*). The fractions containing sylvaticin were mixed, dialyzed against water, adjusted to 5 m*M* sodium acetate/acetic acid pH 6 and loaded onto a Macroprep High Q (Bio-Rad) anion-exchange column pre-equilibrated in 5 m*M* acetate pH 6 buffer. After washing, the protein was eluted with 50 m*M* sodium acetate pH 4. This fraction was adjusted to pH 7 with NaOH and to 20%(*v*/*v*) acetonitrile and then loaded onto a Synchroprep C4 (Synchrom) column. The column was washed with 20% aqueous acetonitrile containing 50 m*M* sodium formate pH 7 and elution achieved by increasing the acetonitrile concentration to 40% in 50 m*M* sodium formate. The fractions containing sylvaticin were pooled, briefly evaporated under vacuum to eliminate acetonitrile, extensively dialysed against ultrapure water and freeze-dried. All purification steps were followed by SDS–PAGE and HPLC as described previously (Le Berre *et al.*, 1994). 5 l of initial culture filtrate produced 150 mg of sylvaticin at homogeneity.

### 2.2. Crystallization

Monoclinic crystals (space group *C*2) of sylvaticin were grown as described previously (Lascombe *et al.*, 2004) in 20%(*v*/*v*) PEG 2000 MME, 0.01 *M* $NiCl_2$ and 0.1 *M* Tris–HCl pH 7.5. Crystals were obtained as very thin imbricated plates ($15 \times 100 \times 200$ µm) containing two molecules (one dimer) in the asymmetric unit. Several cocrystallization assays with sterols were attempted by dissolving an excess of cholesterol in tetrahydrofuran followed by incubation for several hours with a solution of sylvaticin and setting up crystallization after centrifugation. This always resulted in either the previous monoclinic crystals or a new triclinic form with two independent dimers in the asymmetric unit.

### 2.3. X-ray data collection and data processing

Prior to flash-freezing, the crystals were soaked in a cryoprotectant solution containing 20%(*v*/*v*) glycerol.

**2.3.1. Monoclinic crystals**. Diffraction data from these crystals were recorded on beamline BM14 at ESRF (Grenoble). Two data sets were first collected with the intention of attempting S-SAD structure solution ($\lambda = 1.75$ Å). The crystal-to-detector (MAR CCD) distance was set to the minimum value, *i.e.* 75 mm, in order to obtain a reasonable resolution at the detector edge (2.7 Å). In addition, one data set was collected at the tabulated Ni *K*-edge wavelength (1.48 Å), with the aim of recording some anomalous signal up to 2.1 Å resolution from putatively bound Ni atoms, as the presence of nickel chloride was mandatory in order to obtain crystals. No attempt was made to align the crystal and measure Bijvoet-related reflections on the same or even on neighbouring images. It was already known that flash-frozen crystals of sylvaticin could diffract to high resolution (see Lascombe *et al.*, 2004), therefore an additional run was carried out at $\lambda = 1.24$ Å in order to collect a high-resolution data set ($d_{\min} = 1.7$ Å at the edge of the detector, although the limit of diffraction could extend to a higher value). The rationale behind this 'hurried' data-collection strategy was to minimize the effect of non-isomorphism between data sets in case of phase extension to allow complete solution of the structure. All data were integrated with *DENZO* and scaled with *SCALEPACK* (Otwinowski & Minor, 1997) with the *hkl* and reflections in an anomalous pair being treated as separate reflections during both scaling and merging in the latter. Details of this are given in Table 1. For all data sets, mean structure-factor amplitudes and anomalous differences were derived using the program *TRUNCATE* (Collaborative Computational Project, Number 4, 1994; French & Wilson, 1978).

**2.3.2. Triclinic crystals**. Data were collected on the ID14-EH3 beamline at ESRF and were processed using *XDS* (Kabsch, 1993). No anomalous scattering information was taken into account as the structure was planned to be solved

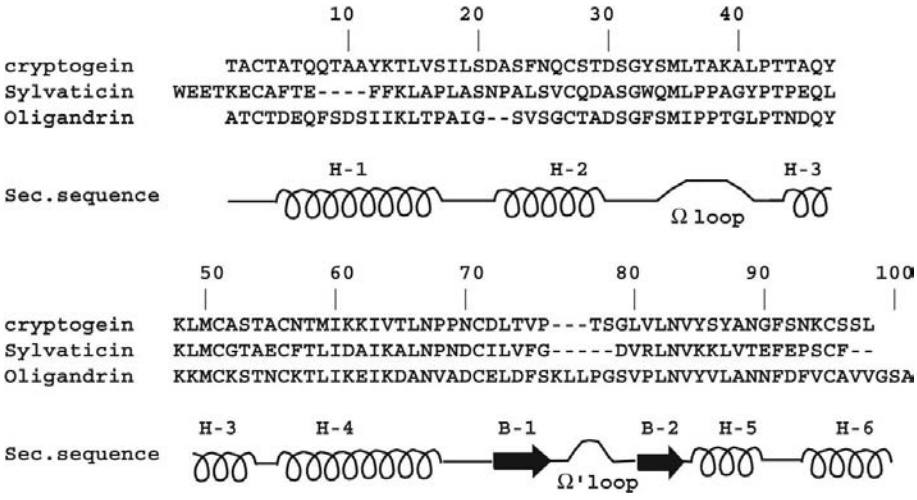


**Figure 1**
Sequence alignment of a $\beta$-elicitin ($\beta$-cryptogein) and the elicitin-like proteins sylvaticin and oligandrin. Labelling is according to cryptogein. The secondary-structure assignment is also described in Fig. 3.

**Table 1**
Data-collection statistics.

Values in parentheses are for the highest resolution shell.

| | Near Ni *K* edge | High-resolution sweep | Native data (second crystal form) |
|---|---|---|---|
| Data collection | | | |
| Beamline (ESRF) | BM14 | BM14 | ID14-EH3 |
| Wavelength (Å) | 1.483 | 1.239 | 0.931 |
| Data-collection temperature (K) | 100 | 100 | 100 |
| Exposure time per frame (s) | 15 | 15 | 10 |
| Angular increment per frame (°) | 1 | 1 | 1 |
| Total rotation range (°) | 110 | 200 | 180 |
| Crystal-to-detector distance (mm) | 75 | 75 | 138 |
| Space group | *C*2 | | *P*1 |
| Unit-cell parameters | | | |
| *a* (Å) | 100.69 | | 36.22 |
| *b* (Å) | 25.97 | | 46.00 |
| *c* (Å) | 68.35 | | 55.73 |
| $\alpha$ (°) | — | | 85.20 |
| $\beta$ (°) | 99.69 | | 71.27 |
| $\gamma$ (°) | — | | 74.63 |
| Data reduction | | | |
| No. of measured reflections (Å) | 45467 | 140835 | 82384 |
| Resolution limits | 30.0–2.07 | 30–1.72 | 33.0–1.60 |
| No. of unique reflections | 10050 | 18321 | 40265 |
| Data completeness (%) | 91.1 (71.8) | 96.4 (68.8) | 92.0 (90.5) |
| Overall $I/\sigma(I)$ | 24.2 (12.5) | 35.3 (11.0) | 18.1 (9.3) |
| Redundancy | 2.3 | 3.9 | 2.0 |
| Overall $R_{\rm sym}$† | 0.048 (0.073) | 0.036 (0.064) | 0.029 (0.073) |

† $R_{\rm sym}$ is defined as $\sum_{hkl}\sum_i |I_i(hkl) - \overline{I_i(hkl)}|/\sum_{hkl}\sum_i I_i(hkl)$, where $I_i(hkl)$ is the intensity of the $i$th observation of reflection $hkl$ and $\langle I(hkl)\rangle$ is the weighted mean of all observations (after rejection of outliers).

by molecular replacement using data from the previous monoclinic form.

### 2.4. Determination of the structure

The structure was investigated using the monoclinic *C*2 form of sylvaticin. Initial attempts to solve the structure either by molecular replacement using $\beta$-cryptogein as a model (PDB code 1beo; Boissy *et al.*, 1996) or by using the S-SAD technique (Dauter *et al.*, 1999) proved unsuccessful.

Nevertheless, investigation of the origin-removed anomalous difference Patterson map calculated using the data collected at $\lambda$ = 1.483 Å (the expected Ni *K*-edge wavelength) confirmed the valuable presence for structure solution of two bound nickel ions in the asymmetric unit. Their coordinates were obtained using *SHELXD* (Schneider & Sheldrick, 2002) and then subjected to heavy-atom refinement and maximum-likelihood-based SAD phasing as implemented in *SHARP* (de La Fortelle & Bricogne, 1997; Bricogne *et al.*, 2003). The correct hand of the heavy-atom subset was selected on the basis of the $E^2$ correlation coefficients obtained after running solvent flattening using *SOLOMON* (Abrahams & Leslie, 1996) on experimental electron-density maps of each hand.

Improved experimental phases were obtained when this data set was combined with the remote-wavelength (1.7 Å resolution) data set and taken as a pseudo-native data set in a SIRAS phase calculation with *SHARP* followed by a density-modification procedure combining *DM* (Cowtan & Main, 1996) and *SOLOMON* for an optimized solvent fraction of 45.4%. Electron-density maps were calculated with *FFT* (Collaborative Computational Project, Number 4, 1994) and displayed using *O* (Jones *et al.*, 1991) *via* the *SHARP* interface. Interpretation of the best solvent-modified density map using the *warpNtrace* procedure (*ARP*/*wARP*; Perrakis *et al.*, 1999) permitted the tracing of 180 peptides out of 188 in two chains with a connectivity index of 0.96 after 50 cycles, this model being refined simultaneously using *REFMAC* (Murshudov *et al.*, 1997).

A post-mortem analysis of the S-SAD data sets collected at 1.75 Å revealed that the sulfur substructure obtained by direct methods using *SHELXD* was only partially correct, showing no contrast between the last correct and the first incorrect peak. The lack of success despite a favourable case (nine S atoms in ~100 residues) was attributed to the unusual shape of the crystal (very thin mica-like imbricated plates), clearly exemplifing what has previously been discussed (Djinović Carugo *et al.*, 2005) regarding absorption corrections in the scaling of strongly anisotropic crystals.

**Table 2**
Refinement statistics.

| | *C*2 | *P*1 |
|---|---|---|
| Total No. of reflections | 17910 | 38238 |
| No. of reflections used for refinement | 16153 | 36214 |
| No. of reflections used for $R_{free}$ | 1757 | 2024 |
| No. of protein atoms | 1459 | 2937 |
| No. of solvent non-H atoms | 16 | 32 |
| No. of water molecules | 225 | 1027 |
| No. of Ni atoms | 2 | 4 |
| No. of Cl atoms | — | 1 |
| Average atomic *B* factors (Å$^2$) | | |
| Protein atoms | 18.5 | 15.6 |
| Solvent molecules | 30.7 | 32.3 |
| Resolution range (Å) | 30–1.72 | 20.0–1.60 |
| *R* value† (%) | 18.57 | 15.00 |
| $R_{free}$‡ (%) | 19.39 | 18.70 |
| Weighted r.m.s.d. from ideality | | |
| Bond lengths (Å) | 0.015 | 0.007 |
| Bond angles (°) | 3.19 | 1.11 |
| Dihedral angles (°) | 25.5 | 23.5 |

† The crystallographic *R* factor is defined as $\sum |F_o| - |F_c| / \sum |F_o|$. ‡ Calculated using 10% (*C*2) and 6% (*P*1) of the native data, which were randomly chosen and excluded from refinement.

The triclinic form of sylvaticin was subsequently solved by molecular replacement from the previously determined *C*2 coordinates using the *Phaser* program (McCoy *et al.*, 2005).

### 2.5. Refinement

Side-chain mutations were performed in compliance with the known sequence of the protein (M. Ponchet, personal communication) and least-squares restrained refinements of the corresponding atomic coordinates and thermal parameters were performed using first *CNSsolve* (Brünger *et al.*, 1998) and then *REFMAC* (Murshudov *et al.*, 1997).

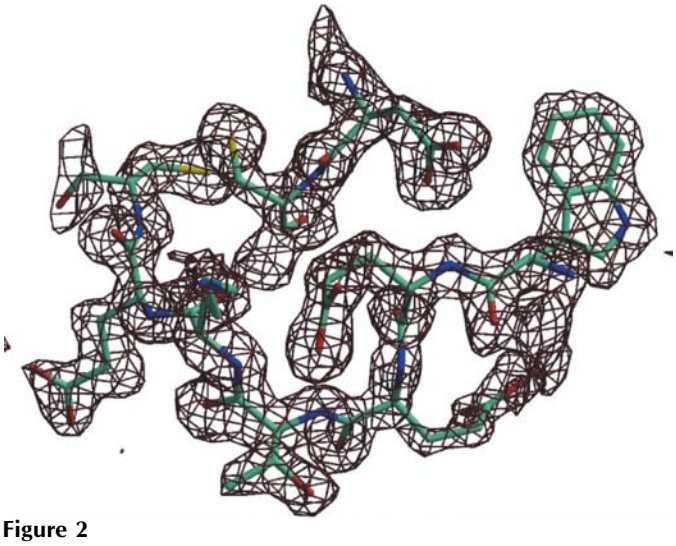

**Figure 2**
Electron-density map of the N-terminal region, including the Cys7–Cys71 disulfide bond and Trp1, of the relevant model at the end of refinement. This map was obtained after experimental Ni-SAD phasing extended to 1.7 Å, followed by density modification in *SOLOMON* and finally the automatic *SHARP*/*ARP*/*wARP*/*REFMAC* procedure. The contour level is 1.2$\sigma$ above mean background.

The final refinement statistics for the monoclinic and triclinic structures are summarized in Table 2.

### 2.6. Structure calculations and analysis

The structure was displayed and analyzed using *O* (Jones *et al.*, 1991) and *Coot* (Emsley & Cowtan, 2004). As evaluated by *PROCHECK* (Laskowski *et al.*, 1993), all nonglycine residues fall within the energetically favourable regions of the Ramachandran plot (Ramachandran *et al.*, 1963). The volumes of the internal cavities of sylvaticin and other elicitins were calculated using the *VOIDOO* software (Kleywegt & Jones, 1994) with a standard probe radius of 1.4 Å. All figures were prepared using *MOLSCRIPT* (Kraulis, 1991), *RASTER3D* (Merritt & Murphy, 1994) and *PyMOL* (DeLano, 2002).

## 3. Results and discussion

### 3.1. Crystallographic model refinement

Fig. 2 displays a region of electron-density map representative of the quality of the initial electron density at the N-terminus of one molecule. The two copies of the model were directly refined at 1.72 Å resolution. 94 amino-acid residues

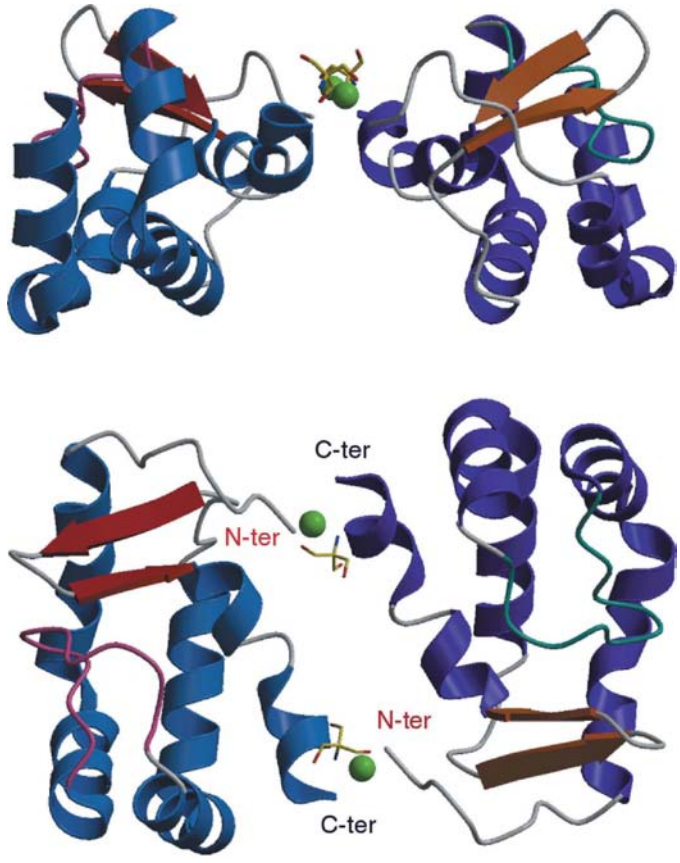


**Figure 3**
Two orthogonal views of ribbon diagrams of the three-dimensional structure of sylvaticin, showing the head-to-tail dimerization of sylvaticin around the two nickel cations (green spheres) in the monoclinic form (the metal-mediated dimer). The same arrangement is also observed in the triclinic crystals.

are incorporated in each molecule, with a small number of highly flexible side chains at the surface which were difficult to trace in the electron density (Lys26, Glu55). Water molecules were gradually introduced during refinement, following the cyclic automated procedure developed in *ARP/wARP* (Perrakis *et al.*, 1999).

### 3.2. Overall structure

Sylvaticin is associated as a dimer in both the *C*2 and *P*1 crystals (Fig. 3). The sylvaticin monomer is built around the three standard disulfide bridges Cys7–Cys71, Cys27–Cys56 and Cys51–Cys93 of the elicitin class. It presents all the structural features of elicitins, with six helices wrapping around a hydrophobic cavity lined by two flexible loops. Each dimer in the crystal is built by head-to-tail association of the N- and C-terminal residues of two single-chain units using two nickel cations (Figs. 3 and 4). In the dimers, the structure of monomeric sylvaticin is rigid and strictly conserved as evidenced from the r.m.s. coordinate differences reported in Table 3. However, comparison of the sylvaticin structure with elicitin structures reveals some important differences. Firstly, sylvaticin presents an unusual hydrophobic patch on the surface opposite the dimer interface. This hydrophobic region is protected from solvent access by self-association through the interaction of several phenylalanine residues (Fig. 5) so that it is not clear which dimer in the crystal is tighter: the dimer built through the polar interfaces (the metal-mediated dimer; Fig. 3) or the dimer built using the hydrophobic surfaces (Fig. 5). The centre-of-mass distances measured between the molecules forming each dimer do not solve this problem, as they are nearly identical (28.2 Å for the former association and 27.2 Å for the latter). Secondly, superimposition of the cryptogein and sylvaticin structures (Fig. 6) shows that the orientations and lengths of the helices and loops are different, especially helix H1, which reduces the size of the cavity, also explaining why initial attempts to solve the structure by molecular replacement were unsuccessful.

**Table 3**
R.m.s.d. values between equivalent positions of each monomer from the *P*1 and *C*2 structures using *P*1 sylvaticin chain *A* as the reference chain.

| R.m.s. difference (Å) | All atoms | Main-chain atoms | Side-chain atoms |
|---|---|---|---|
| *P*1 chain *B* | 0.62 | 0.35 | 0.82 |
| *P*1 chain *C* | 0.67 | 0.40 | 0.86 |
| *P*1 chain *D* | 0.67 | 0.40 | 0.86 |
| *C*2 chain *A* | 0.78 | 0.32 | 1.06 |
| *C*2 chain *B* | 0.89 | 0.40 | 1.20 |

### 3.3. Bound nickel and other solvent molecules

Although not related to any particular biological function, Ni atoms were found to be mandatory for crystallization, as well as the use of Tris buffer to obtain crystals of good quality. It is not surprising that these two moieties were found ordered in the crystal structure. Fig. 4 shows the arrangement around one of the two Ni atoms. Each of them is tightly bonded to the N- and C-termini of two molecules arranged head-to-tail and completes its sphere of coordination with a Tris ion and a water molecule. As such, these two features, the Ni atoms (playing the role of a 'glue') and the hydrophobic patch on the other side (auto-association), both participate in the formation and the stability of suitable crystals able to diffract to high resolution.

### 3.4. Description of the cavity

To achieve the transport of sterols and other lipids, 'standard' elicitins possess a large internal hydrophobic cavity that is specific for phytosterols such as ergosterol, but that can also accommodate cholesterol (Lascombe *et al.*, 2000; Rodrigues *et al.*, 2006) with a $K_m$ value in the micromolar range. This cavity is lined internally by a large number of hydrophobic residues, with the exception of the polar Tyr47 located at the bottom of the cavity (in $\beta$-elicitins), which is essential for binding as it is

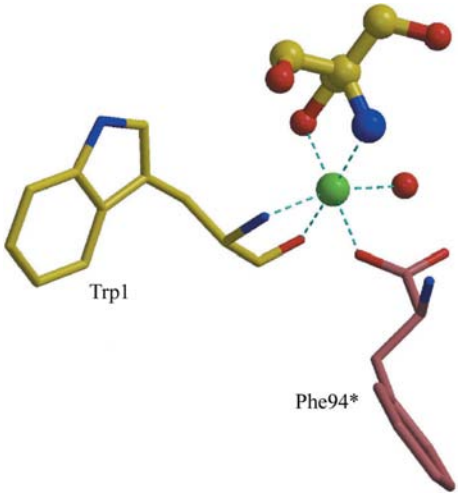


**Figure 4**
The surroundings of the nickel ion. A molecule of Tris (buffer) and a water molecule complete the tight hexacoordination of each nickel cation (the dashed distances are in the range 2.03–2.26 Å).

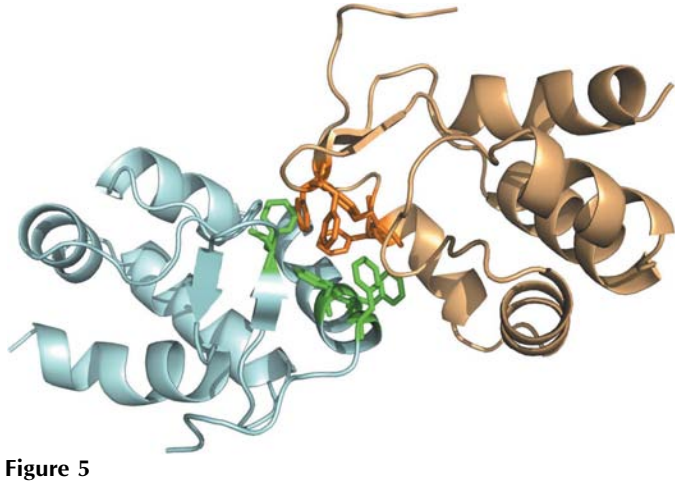

**Figure 5**
The hydrophobic interface between two adjacent sylvaticin dimers (the hydrophobic dimer). The packing contacts between the two neighbours involve eight phenylalanine side chains (Phe9, Phe12, Phe13, Phe75 and their symmetry-related mates).

hydrogen-bonded to the 3-OH of the sterol. When a chloride or a bromide ion replaces the sterol 3$\beta$-hydroxyl group, no complexation occurs. The way that elicitins trap and release their ligand remains uncertain despite several molecular-simulation studies (Demaret *et al.*, 2000). The volume of the cavity changes drastically compared with the free unliganded protein. In the case of cryptogein–cholesterol, the volume is 290 Å$^3$ in the complex and reduces to ∼20–30 Å$^3$ in the unliganded protein. The way the cavity expands is the result of specific inner side-chain rotations that produce room for the sterol. In addition, the two loops Ω and Ω′ that form the lid of the cavity allow the capture and release of the sterol. Interestingly, the main-chain scaffolding of the cavity remains nearly identical in complexed and uncomplexed cryptogein (r.m.s.d. = 1.01 Å), revealing a smooth capture and release mechanism, thus leading standard elicitins to be nicknamed 'phytosterol shuttles'. The situation in sylvaticin is different owing to a number of structural modifications: firstly, the bulky Trp33 residue points inwards into the cavity, in addition to several other hydrophobic side chains that are oriented accordingly (Leu15, Leu24, Leu36, Leu47, Leu80, Leu85 and Met35), and secondly, Tyr47 is missing and cannot provide the specific polar interaction with the 3$\beta$ hydroxyl group of the sterol (in sylvaticin, this key residue is replaced by a leucine). Under these conditions, no cavity can be detected in the first subunit of the dimer, while a small meaningless cavity of 6–7 Å$^3$ exists in the second subunit. These features certainly explain why all attempts to prepare a cholesterol complex, which can be easily formed by the two $\beta$-elicitins cryptogein and cinnamomin, were unsuccessful in the case of sylvaticin. No cholesterol could be observed in any electron-density map resulting from complexation trials of sylvaticin and cholesterol.

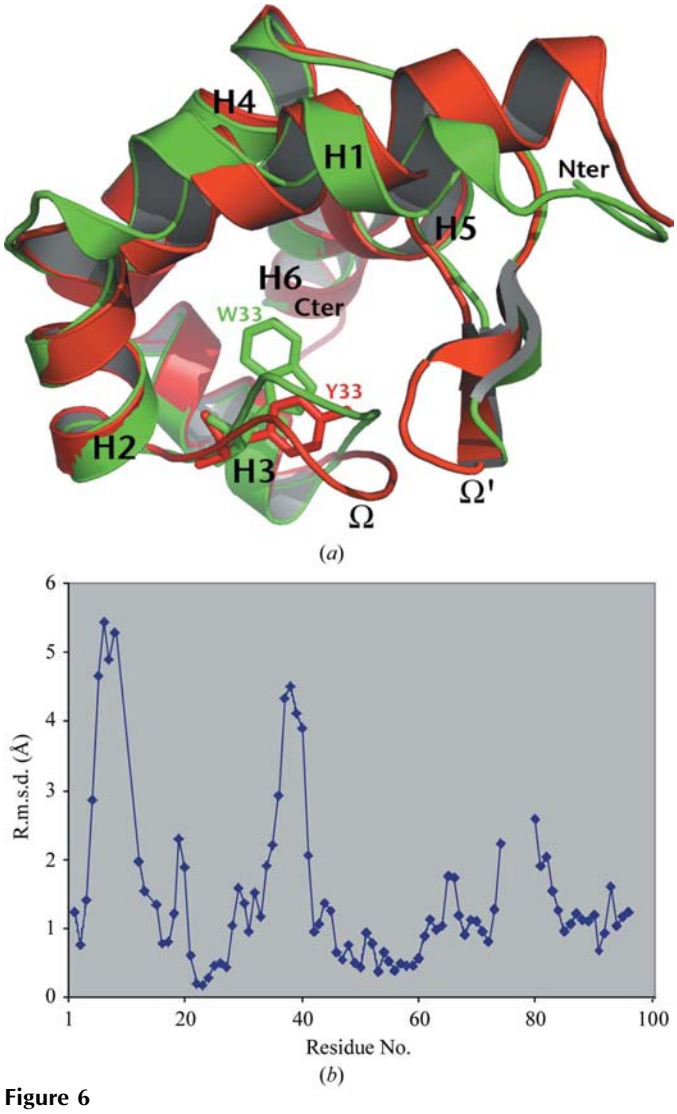


**Figure 6**
(*a*) Superimposition of sylvaticin (green) and cryptogein (red), showing the differences between the two proteins. In sylvaticin, helix H1 delimits a narrower cavity than in cryptogein. The Trp33 residue (which replaces Tyr33) is oriented inwards into the cavity. (*b*) Least-squares superimposition of the main-chain atoms of free $\beta$-cryptogein and sylvaticin plotted against sequence number. The gap 77–82 arises from the different lengths of the respective Ω′ loops.

### 3.5. Biological activity and structure relationship

The present two structures show dimers of sylvaticin as the crystallographic asymmetric unit. There is no evidence that this oligomerization represents the biologically active molecule; all experimental assays, including native gels, suggest that the monomer is actually the true functional and active unit. Furthermore, the monomer three-dimensional structure built around the three disulfide bridges is sufficiently well characterized to be a realistic description of the active monomer in solution.

Considerable interest has been devoted to elicitins because of their properties as a new generation of potent biological pest-control agents. The bioactivity of these vectors is a balance between the beneficial systemic acquired resistance (SAR; induced *in planta* against further pathogen attacks) and the toxic hypersensitive response (HR). Of the elicitins so far investigated, the $\alpha$-series usually induce a much lower toxicity than the $\beta$-series. Sylvaticin, which is closely related to oligandrin, appears to be the most promising $\alpha$-series pythin, although its SAR is slightly lower.

It has been demonstrated that the complexation of elicitins with sterols is a prerequisite to trigger the biological response of elicitins (Mikes *et al.*, 1998; Osman *et al.*, 2001). Although the gross structures are similar in sylvaticin and cryptogein or other elicitins, superimpositions of the main chains differ (comparisons and r.m.s.d.s are reported in Fig. 5), with a special mention of the lid of the cavity (the Ω and Ω′ loops). The lack of Tyr47, which is mandatory for sterol binding, is probably the most important feature that may distinguish sylvaticin from elicitins, but may not be crucial, as another residue, Tyr41, in the vicinity could play the same role following a rotation, with the express condition that Trp33 can find its way out of the cavity. This structural information may provide the reason why sterol cannot be included in the crystal. Spectroscopic evidence indicates that sylvaticin still interacts with sterols in solution like other elicitins; however, there is no indication of the exact nature of these interactions.

They may proceed either through the central cavity or with the hydrophobic patch at the surface that covers about 400 Å$^2$ (two times the sterol surface) and at the origin of the dimerization in the crystal.

In this context, we cannot ascertain whether sylvaticin shares all the biochemical properties of standard elicitins and whether the triggering of the HR/SAR biological mechanisms would follow the same or a different pathway than that observed for 'standard' elicitins.

## 4. Conclusions and perspectives

Even though the cavity in sylvaticin does not share all the properties observed for $\beta$-cryptogein, the three-dimensional structure of this small pythin protein shows that it is closely related to $\alpha$-elicitins, with similar folding and disulfide bridges. However, when compared with those of elicitins its X-ray structure shows a number of structural differences; in particular, it possesses a number of bulky residues (Trp) that limit the access of phytosterols and lipids to the central cavity and the two $\Omega$ and $\Omega'$ loops lining the cavity are more extended and as such would modify the selectivity of the putative capture. How this protein acts in the pathology triggered by *P. sylvaticum* still remains to be analyzed.

We are grateful to the European Synchrotron Radiation Facility (ESRF) in Grenoble and Martin Walsh for beam time and assistance during data collection. We thank Globalphasing Ltd for licenses for *SHARP* and *autoSHARP*. PR was supported by European commission grant No. HPRI-CT-1999-50015 within the EXMAD project.

## References

Abrahams, J. P. & Leslie, A. G. W. (1996). *Acta Cryst.* D**52**, 30–42.
Benhamou, N., Belanger, R. R., Rey, P. & Tirilly, Y. (2001). *Plant Physiol. Biochem.* **39**, 681–696.
Bonnet, P., Bourdon, E., Ponchet, M., Blein, J. P. & Ricci, P. (1996). *Eur. Plant Pathol.* **102**, 181–192.
Boissy, G., de La Fortelle, E., Kahn, R., Huet, J. C., Bricogne, G., Pernollet, J. C. & Brunie, S. (1996). *Structure*, **4**, 1429–1439.
Boissy, G., O'Donohue, M., Gaudemer, O., Perez, V., Pernollet, J. C. & Brunie, S. (1999). *Protein Sci.* **8**, 1191–1199.
Bricogne, G., Vonrhein, C., Flensburg, C., Schiltz, M. & Paciorek, W. (2003). *Acta Cryst.* D**59**, 2023–2030.
Brünger, A. T., Adams, P. D., Clore, G. M., DeLano, W. L., Gros, P., Grosse-Kunstleve, R. W., Jiang, J.-S., Kuszewski, J., Nilges, M., Pannu, N. S., Read, R. J., Rice, L. M., Simonson, T. & Warren, G. L. (1998). *Acta Cryst.* D**54**, 905–921.
Collaborative Computational Project, Number 4 (1994). *Acta Cryst.* D**50**, 760–763.
Cowtan, K. D. & Main, P. (1996). *Acta Cryst.* D**52**, 43–48.
Dauter, Z., Dauter, M., de La Fortelle, E., Bricogne, G. & Sheldrick, G. M. (1999). *J. Mol. Biol.* **289**, 83–92.
DeLano, W. L. (2002). *PyMOL*. DeLano Scientific, San Carlos, CA, USA.
Demaret, S., Demaret, J. P. & Brunie, S. (2000). *J. Biol. Struct. Dyn.* **18**, 453–460.
Djinović Carugo, K., Helliwell, J. R., Stuhrmann, H. & Weiss, M. S. (2005). *J. Synchrotron Rad.* **12**, 410–419.
Emsley, P. & Cowtan, K. (2004). *Acta Cryst.* D**60**, 2126–2132.
Fefeu, S., Bouaziz, S., Huet, J. C., Pernollet, J. C. & Guittet, E. (1997). *Protein Sci.* **6**, 2279–2284.
French, S. & Wilson, K. (1978). *Acta Cryst.* A**34**, 517–525.
Gooley, P. R., Keniry, M. A., Dimitrov, R. A., Marsh, D. E., Keizer, D. W., Gayler, K. R. & Grant, B. R. (1998). *J. Biomol. NMR*, **12**, 523–534.
Huet, J. C., Le Caer, J. P., Nespoulous, C. & Pernollet, J. C. (1995). *Mol. Plant Microb. Interact.* **8**, 302–310.
Jones, T. A., Zou, J.-Y., Cowan, S. W. & Kjeldgaard, M. (1991). *Acta Cryst.* A**47**, 110–119.
Kabsch, W. (1993). *J. Appl. Cryst.* **26**, 795–800.
Kleywegt, G. J. & Jones, T. A. (1994). *Acta Cryst.* D**50**, 178–185.
Kraulis, P. J. (1991). *J. Appl. Cryst.* **24**, 946–950.
La Fortelle, E. de & Bricogne, G. (1997). *Methods Enzymol.* **276**, 472–494.
Lascombe, M.-B., Milat, M.-L., Blein, J.-P., Panabières, F., Ponchet, M. & Prangé, T. (2000). *Acta Cryst.* D**56**, 1498–1500.
Lascombe, M.-B., Ponchet, M., Cardin, L., Milat, M.-L., Blein, J.-P. & Prangé, T. (2004). *Acta Cryst.* D**60**, 362–364.
Lascombe, M.-B., Ponchet, M., Venard, P., Milat, M.-L., Blein, J.-P. & Prangé, T. (2002). *Acta Cryst.* D**58**, 1442–1447.
Laskowski, R. A., MacArthur, M. W., Moss, D. S. & Thornton, J. M. (1993). *J. Appl. Cryst.* **26**, 283–291.
Le Berre, J., Panabières, F., Ponchet, M., Denoroy, L., Bonnet, P., Marais, A. & Ricci, P. (1994). *Plant Physiol. Biochem.* **32**, 1–5.
Le Floch, G., Benhamou, N., Mamaca, E., Salerno, M. I., Tirilly, Y. & Rey, P. (2005). *Plant Physiol. Biochem.* **43**, 1–11.
McCoy, A. J., Grosse-Kunstleve, R. W., Storoni, L. C. & Read, R. J. (2005). *Acta Cryst.* D**61**, 458–464.
Merritt, E. A. & Murphy, M. E. P. (1994). *Acta Cryst.* D**50**, 869–873.
Mikes, V., Milat, M. L., Ponchet, M., Panabières, F., Ricci, P. & Blein, J. P. (1998). *Biochem. Biophys. Res. Commun.* **245**, 133–139.
Mikes, V., Milat, M. L., Ponchet, M., Ricci, P. & Blein, J. P. (1997). *FEBS Lett.* **4**, 190–192.
Murshudov, G. N., Vagin, A. A. & Dodson, E. J. (1997). *Acta Cryst.* D**53**, 240–255.
Osman, H., Vauthrin, S., Mikes, V., Milat, M. L., Panabières, F., Marais, A., Brunie, S. & Maume, B. (2001). *Mol. Biol. Cell*, **12**, 2825–2834.
Otwinowski, Z. & Minor, W. (1997). *Methods Enzymol.* **276**, 306–326.
Panabières, F., Ponchet, M., Allasia, V., Cardin, L. & Ricci, P. (1997). *Mycol. Res.* **101**, 1459–1468.
Perrakis, A., Morris, R. J. & Lamzin, V. S. (1999). *Nature Struct. Biol.* **6**, 458–463.
Picard, K., Ponchet, M., Blein, J. P., Rey, P., Tirilly, Y. & Benhamou, N. (2000). *Plant Physiol.* **124**, 379–395.
Ponchet, M., Panabières, F., Milat, M. L., Mikes, V., Montillet, J. L., Suty, L., Triantaphylides, C., Tirilly, Y. & Blein, J. P. (1999). *Cell Mol. Life Sci.* **56**, 1020–1047.
Ramachandran, G. N., Ramakrishnan, C. & Sasisekharan, V. (1963). *J. Mol. Biol.* **7**, 95–99.
Rodrigues, M. L., Archer, M., Martel, P., Jacquet, A., Cravador, A. & Carrondo, M. A. (2002). *Acta Cryst.* D**58**, 1314–1321.
Rodrigues, M. L., Archer, M., Martel, P., Miranda, S., Thomaz, M., Enguita, F. J., Baptista, R. P., Pinho e Melo, E., Sousa, N., Cravador, A. & Carrondo, M. A. (2006). *Biophys. Biochim. Acta*, **1764**, 110–121.
Schneider, T. R. & Sheldrick, G. M. (2002). *Acta Cryst.* D**58**, 1772–1779.
Wang, P. H. & White, J. G. (1997). *Physiol. Mol. Plant Pathol.* **51**, 129–143.